

Article

# Reaction Mechanisms of CO<sub>2</sub> Reduction to Formaldehyde Catalyzed by Hourglass Ru, Fe, and Os Complexes: A Density Functional Theory Study

Chunhua Dong<sup>1,2,3</sup>, Mingsong Ji<sup>1</sup>, Xinzheng Yang<sup>1,\*</sup>, Jiannian Yao<sup>2</sup> and Hui Chen<sup>2,\*</sup>

<sup>1</sup> Beijing National Laboratory for Molecular Sciences, State Key Laboratory for Structural Chemistry of Unstable and Stable Species, Institute of Chemistry, Chinese Academy of Sciences, Beijing 100190, China; dongchunhua@iccas.ac.cn (C.D.); lhjms@iccas.ac.cn (M.J.)

<sup>2</sup> Beijing National Laboratory for Molecular Sciences, CAS Key Laboratory of Photochemistry, Institute of Chemistry, Chinese Academy of Sciences, Beijing 100190, China; jnyao@iccas.ac.cn

<sup>3</sup> College of Chemistry, Chemical Engineering and Material, Handan Key Laboratory of Organic Small Molecule Materials, Handan University, Handan 056005, China

\* Correspondence: xyang@iccas.ac.cn (X.Y.); chen@iccas.ac.cn (H.C.); Tel.: +86-10-8236-2928 (X.Y.); +86-10-6256-1749 (H.C.)

Academic Editors: Albert Demonceau, Ileana Dragutan and Valerian Dragutan

Received: 23 September 2016; Accepted: 21 December 2016; Published: 27 December 2016

**Abstract:** The reaction mechanisms for the reduction of carbon dioxide to formaldehyde catalyzed by bis(tricyclopentylphosphine) metal complexes, [RuH<sub>2</sub>(H<sub>2</sub>)(PCyp<sub>3</sub>)<sub>2</sub>] (**1<sub>Ru</sub>**), [FeH<sub>2</sub>(H<sub>2</sub>)(PCyp<sub>3</sub>)<sub>2</sub>] (**1<sub>Fe</sub>**) and [OsH<sub>4</sub>(PCyp<sub>3</sub>)<sub>2</sub>] (**1<sub>Os</sub>**), were studied computationally by using the density functional theory (DFT). **1<sub>Ru</sub>** is a recently reported highly efficient catalyst for this reaction. **1<sub>Fe</sub>** and **1<sub>Os</sub>** are two analogues of **1<sub>Ru</sub>** with the Ru atom replaced by Fe and Os, respectively. The total free energy barriers of the reactions catalyzed by **1<sub>Ru</sub>**, **1<sub>Fe</sub>** and **1<sub>Os</sub>** are 24.2, 24.0 and 29.0 kcal/mol, respectively. With a barrier close to the experimentally observed Ru complex, the newly proposed iron complex is a potential low-cost catalyst for the reduction of carbon dioxide to formaldehyde under mild conditions. The electronic structures of intermediates and transition states in these reactions were analyzed by using the natural bond orbital theory.

**Keywords:** reaction mechanism; carbon dioxide; formaldehyde; homogeneous catalysis; ruthenium; iron; osmium

## 1. Introduction

As an abundant and non-toxic C<sub>1</sub>-building block, carbon dioxide can be reduced to various chemicals, such as carbon monoxide [1], methanol [2], formaldehyde [3], acetals [4,5], formic acid [5], formate [6,7], formamides [8], methylamines [8], formamidines [8], imines [3] and methane [9]. Recently, Beller and co-workers [10] reported the methylation of aromatic C–H bonds using CO<sub>2</sub> and H<sub>2</sub> with the assistance of a ruthenium triphos catalyst. In addition to the experimental studies, there are some theoretical studies on catalytic reduction of CO<sub>2</sub> in recent years. Pidko [11] used a bis-N-heterocyclic carbene ruthenium CNC-pincer as catalyst and studied the mechanism of CO<sub>2</sub> hydrogenation to formates by DFT method. Haunschild [12] reported the catalytic reduction of carbon dioxide to methanol by using (Triphos)Ru(TMM) as catalyst. Musashi and Sakaki [13] reported a theoretical study of *cis*-RuH<sub>2</sub>(PH<sub>3</sub>)<sub>4</sub>-catalyzed hydrogenation of CO<sub>2</sub> into formic acid.

As mild reducing agents, boron-containing compounds have been widely used in carbon dioxide reduction [14,15]. Hazari and co-workers [16] reported the allene carboxylation with CO<sub>2</sub> using a PSiP pincer ligand supported palladium complex as the catalyst in the hydroboration of CO<sub>2</sub>. Maron and co-workers [17,18] reported the phosphine–borane-mediated hydroboration of CO<sub>2</sub> to methanol using

an organocatalyst 1-Bcat-2-PPh<sub>2</sub>-C<sub>6</sub>H<sub>4</sub> (Bcat = catecholboronyl). Their mechanistic study showed that the simultaneous activation of both the reducing agent and CO<sub>2</sub> plays an important role in the catalytic reaction. Bouhadir and co-workers [19] reported the hydroboration of CO<sub>2</sub> to methoxyboranes with the ambiphilic phosphine–borane derivatives as catalysts. They also demonstrated that the formaldehyde adducts are indeed the actual catalyst in the reaction. Wegner and co-workers [20] reported a selective reduction of CO<sub>2</sub> to methanol using Li<sub>2</sub>[1,2-C<sub>6</sub>H<sub>4</sub>(BH<sub>3</sub>)<sub>2</sub>] as the catalyst with the presence of pinacolborane. Their work shows a novel transition-metal-free mode in which the aromaticity plays an important role in the bidentate activation process.

Given the above progress, we can see that the reduction of carbon dioxide to formic acid and its derivatives has been well studied. However, as a key step in the production of methanol from CO<sub>2</sub> and H<sub>2</sub>, the catalytic reduction of CO<sub>2</sub> to formaldehyde is rarely reported. Huang et al. [21] studied the mechanistic details of nickel pincer-catalyzed reduction of CO<sub>2</sub> to a methanol derivative with catecholborane (HBcat), and found that formaldehyde is an inevitable intermediate, although it was not observed in the experiment. Hazari and co-workers [22] reported a CO<sub>2</sub> reduction reaction using a nickel  $\eta^3$ -cyclooctenyl complex supported by tridentate PSiP pincer ligand as the precatalyst, and detected the characteristic peak (8.72 ppm) of formaldehyde in a <sup>1</sup>H-NMR spectrum. However, the formaldehyde was mixed with miscellaneous unverifiable products without a clear yield. Hill and co-workers [23] reported a selective reductive hydroboration of CO<sub>2</sub> to a methanol equivalent, CH<sub>3</sub>OBpin, using B(C<sub>6</sub>F<sub>5</sub>)<sub>3</sub>-activated alkaline earth compounds as catalysts. They also proposed a mechanism with the formation of formaldehyde as a byproduct. Tzschucke and co-workers [24] reported an electrocatalytic reduction of CO<sub>2</sub> to formic acid and found an occasional formation of formaldehyde using bipyridine iridium complexes with pentamethylcyclopentadienyl ligands as the catalysts. In the above reactions, formaldehyde was only observed as byproducts with extremely low yields.

In 2014, Bontemps and co-workers [3] reported the first unambiguous detection of formaldehyde from the pinacolborane reduction of CO<sub>2</sub> with a yield of 22% using the dihydride bis(dihydrogen) bis(tricyclopentylphosphine) hourglass ruthenium complex [RuH<sub>2</sub>(H<sub>2</sub>)<sub>2</sub>(PCyp<sub>3</sub>)<sub>2</sub>] (**Ru-1cyp**) as the catalyst precursor at room temperature in 24 h. Although the selectivity and yield of formaldehyde are not ideal enough, the controllable generation of formaldehyde by reducing CO<sub>2</sub> is still a significant breakthrough. However, detailed mechanism of the above reaction, such as the structures of rate-limiting states, is still missing. In this paper, we report a density functional theory (DFT) study of the reaction mechanisms of the reduction of CO<sub>2</sub> to formaldehyde catalyzed by [RuH<sub>2</sub>(H<sub>2</sub>)<sub>2</sub>(PCyp<sub>3</sub>)<sub>2</sub>] (**1<sub>Ru</sub>**) and its Fe and Os analogues, [FeH<sub>2</sub>(H<sub>2</sub>)<sub>2</sub>(PCyp<sub>3</sub>)<sub>2</sub>] (**1<sub>Fe</sub>**) and [OsH<sub>4</sub>(PCyp<sub>3</sub>)<sub>2</sub>] (**1<sub>Os</sub>**). The potentials of **1<sub>Fe</sub>** and **1<sub>Os</sub>** as catalysts for the reaction were predicted accordingly. The relations between the electronic structures and catalytic properties were analyzed using the natural bond orbital (NBO) theory [25].

## 2. Results and Discussion

### 2.1. The Mechanism for the Reduction of Carbon Dioxide to Formaldehyde Catalyzed by the Ru Complex

Scheme 1 shows the whole catalytic cycle for the reduction of carbon dioxide to formaldehyde catalyzed by **1<sub>Ru</sub>**. Figure 1 shows the corresponding free energy profile. Figure 2 shows the optimized structures of transition states in the catalytic cycle.

At the beginning of the reaction, the dissociation of H<sub>2</sub> from **Ru-1cyp** forms the 10.5 kcal/mol less stable catalyst [RuH<sub>2</sub>(H<sub>2</sub>)<sub>2</sub>(PCyp<sub>3</sub>)<sub>2</sub>] (**1<sub>Ru</sub>**), which could attract a HBpin molecule and form a 15.8 kcal/mol more stable intermediate **1<sub>Ru-HBpin</sub>**. The exchange of CO<sub>2</sub> with HBpin in **1<sub>Ru-HBpin</sub>** for the formation of **2<sub>Ru</sub>** is 14.8 kcal/mol uphill. Next, **3<sub>Ru</sub>** is formed through transition state **TS<sub>2,3-Ru</sub>** with a 5.5 kcal/mol barrier for the transfer of a hydride from Ru to the carbon in CO<sub>2</sub>. The newly formed formate group in **3<sub>Ru</sub>** could easily rearrange through **TS<sub>3,4-Ru</sub>** and **TS<sub>4,5-Ru</sub>** for the formation of a more stable intermediate **5<sub>Ru</sub>**. Then, a HBpin molecule attacks **5<sub>Ru</sub>** and forms a 2.6 kcal/mol less stable intermediate **6<sub>Ru</sub>** with a weak interaction between O and B. Next, **7<sub>Ru</sub>** is formed quickly

through  $TS_{6,7-Ru}$  with the stretching of the B–H bond and the formation of the O–B and Ru–H bonds. A pinBOCHO molecule is formed with the cleavage of the Ru–O bond through transition state  $TS_{7,8-Ru}$ , which is 12.2 kcal/mol higher than  $7_{Ru}$  in free energy. The dissociation of pinBOCHO from  $8_{Ru}$  for the regeneration of  $1_{Ru}$  is 1.1 kcal/mol downhill. Then the dissociated pinBOCHO molecule can come back to  $1_{Ru}$  and take a hydride from Ru to its carbonyl carbon for the formation of  $10_{Ru}$  ( $\Delta G^\circ = -8.3$  kcal/mol). After a structural relaxation,  $10_{Ru}$  transforms to a 5.9 kcal/mol more stable intermediate  $11_{Ru}$ . Then a formaldehyde molecule forms with the formation of the Ru–OBpin bond and the breaking of the Ru–OCH<sub>2</sub>OBpin and C–OBpin bonds through transition state  $TS_{11,12-Ru}$ , which is 3.8 kcal/mol higher than  $11_{Ru}$  in free energy. The release of formaldehyde from  $12_{Ru}$  for the formation of  $13_{Ru}$  is 3.0 kcal/mol downhill. Next, another HBpin molecule approaches  $13_{Ru}$  and forms a much more stable intermediate  $15_{Ru}$  with the formation of the B–O bond through  $TS_{14,15-Ru}$ . The Ru–O and H–B bonds in  $15_{Ru}$  could break easily with the formation of a Ru–H bond through  $TS_{15,16-Ru}$ , which is only 4.5 kcal/mol higher than  $15_{Ru}$  in free energy. Then the dissociation of pinBOBpin from  $16_{Ru}$  regenerates  $1_{Ru}$  and completes the catalytic cycle. It is worth noting that HBpin can also attack  $10_{Ru}$  and form a stable acetal compound (pinBO)<sub>2</sub>CH<sub>2</sub>, which was observed in the experiment.

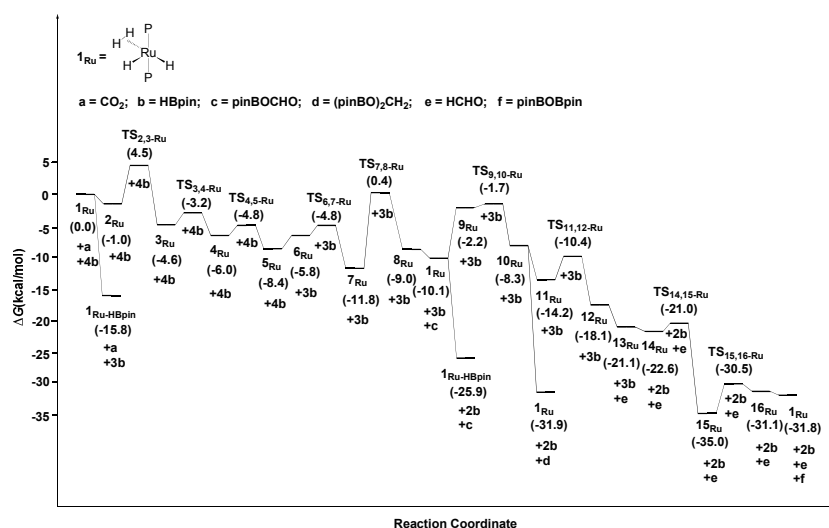


**Figure 1.** Free energies profile of the reduction of carbon dioxide to formaldehyde catalyzed by  $1_{Ru}$ .

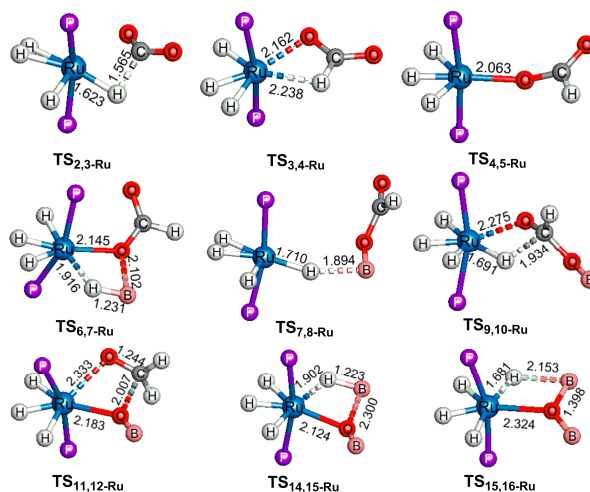
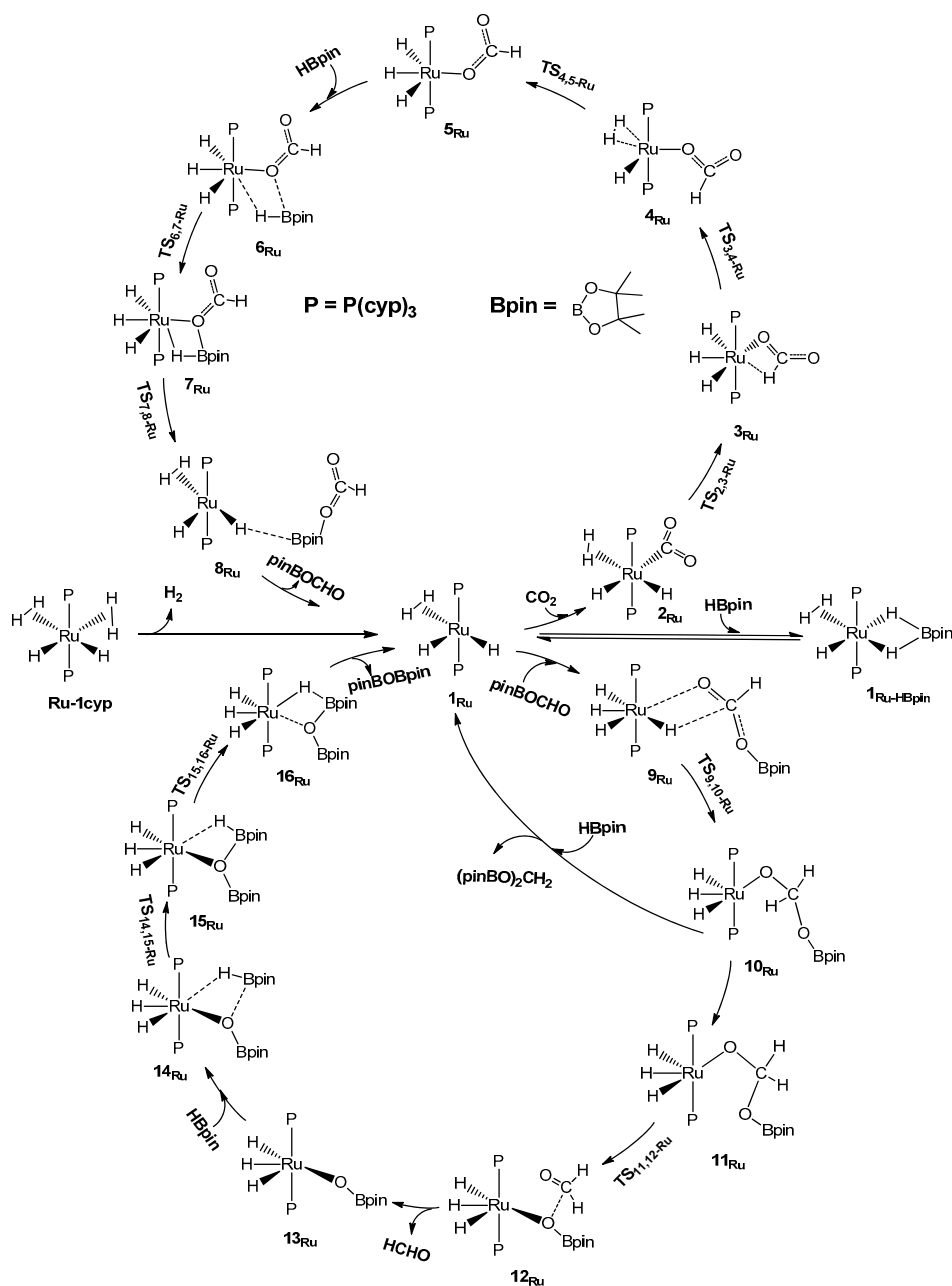


**Figure 2.** Optimized structures of  $TS_{2,3-Ru}$  ( $513i$   $cm^{-1}$ ),  $TS_{3,4-Ru}$  ( $170i$   $cm^{-1}$ ),  $TS_{4,5-Ru}$  ( $176i$   $cm^{-1}$ ),  $TS_{6,7-Ru}$  ( $127i$   $cm^{-1}$ ),  $TS_{7,8-Ru}$  ( $209i$   $cm^{-1}$ ),  $TS_{9,10-Ru}$  ( $363i$   $cm^{-1}$ ),  $TS_{11,12-Ru}$  ( $159i$   $cm^{-1}$ ),  $TS_{14,15-Ru}$  ( $67i$   $cm^{-1}$ ) and  $TS_{15,16-Ru}$  ( $97i$   $cm^{-1}$ ). Bond lengths are in Å. The cyclopentyl and pinacol groups are not shown for clarity.

By comparing all relative free energies shown in Figure 1, we can conclude that  $1_{\text{Ru-HBpin}}$  and  $\text{TS}_{9,10-\text{Ru}}$  are the rate-determining states of the catalytic reaction with a total free energy barrier of 24.2 kcal/mol, which agrees well with the observed experimental reaction rate.

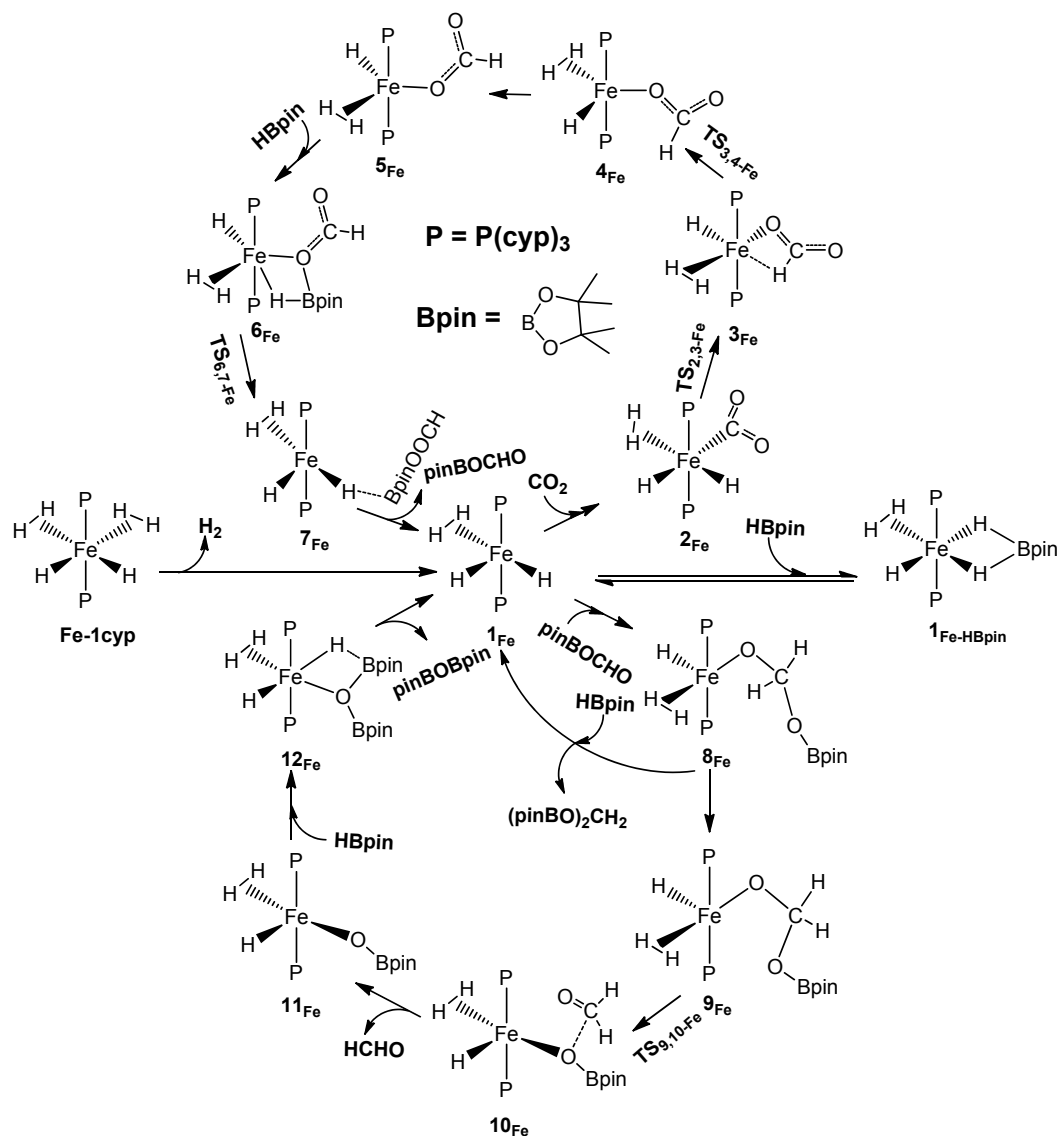
Compared with the mechanism proposed by Huang et al. for the reduction reaction of  $\text{CO}_2$  to a methanol derivative with catecholborane (HBcat) catalyzed by a pincer nickel complex [21], the catalytic reduction of carbon dioxide to formaldehyde reactions catalyzed by hourglass ruthenium complex and pincer nickel complex have similar but not exactly the same pathways. There are two oxygen atoms as possible bonding sites for HBpin in the nickel formate. However, there is only one oxygen atom as the bonding site for HBpin in the ruthenium formate ( $5_{\text{Ru}}$  to  $6_{\text{Ru}}$  in Scheme 1). Our calculations indicate that the six-membered ring structure is less likely to be formed in the hourglass ruthenium complexes.



**Scheme 1.** Catalytic cycle for the reduction of carbon dioxide to formaldehyde catalyzed by  $1_{\text{Ru}}$ .

## 2.2. The Mechanism for the Reduction of Carbon Dioxide to Formaldehyde Catalyzed by the Fe Complex

Scheme 2 shows the whole catalytic cycle for the reduction of carbon dioxide to formaldehyde catalyzed by the newly proposed Fe complex  $1_{\text{Fe}}$ . Figures 3 and 4 show the corresponding free energy profile and optimized structures of key transition states, respectively. The reactions catalyzed by  $1_{\text{Fe}}$  and  $1_{\text{Ru}}$  have similar pathways but different rate-determining states.



**Scheme 2.** Catalytic cycle for the reduction of carbon dioxide to formaldehyde catalyzed by  $1_{\text{Fe}}$ .

Similar to the reaction catalyzed by  $1_{\text{Ru}}$ , a  $-22.0$  kcal/mol more stable intermediate  $1_{\text{Fe-HBpin}}$  is formed at the beginning of the reaction catalyzed by  $1_{\text{Fe}}$ . The exchange of  $\text{CO}_2$  with HBpin in  $1_{\text{Fe-HBpin}}$  and the formation of  $2_{\text{Fe}}$  is  $16.4$  kcal/mol uphill. Next,  $3_{\text{Fe}}$  is formed quickly through transition state  $\text{TS}_{2,3-\text{Fe}}$  for the formation of C–H bond and the rearrangement of hydrogen atoms. The rearrangement of the newly formed formate group and hydrogen atoms in  $3_{\text{Fe}}$  forms a slightly more stable intermediate  $4_{\text{Fe}}$ . After a structural relaxation,  $4_{\text{Fe}}$  transforms to a  $2.0$  kcal/mol more stable intermediate  $5_{\text{Fe}}$ , which attracts a HBpin molecule for the formation of a  $3.9$  kcal/mol more stable intermediate  $6_{\text{Fe}}$  with strong Fe–H and O–B interactions. Then,  $7_{\text{Fe}}$  is formed through a transition state  $\text{TS}_{6,7-\text{Fe}}$  with a free energy barrier of  $20.8$  kcal/mol with the breaking of the Fe–O and B–H bonds and the formation of the O–B bond.  $7_{\text{Fe}}$  is  $12.3$  kcal/mol less stable than  $6_{\text{Fe}}$  with a weak interaction

between H and B. The dissociation of pinBOCHO from  $7_{\text{Fe}}$  for the regeneration of  $1_{\text{Fe}}$  is 3.6 kcal/mol downhill. Next, the dissociated pinBOCHO molecule comes back to  $1_{\text{Fe}}$  and forms a Fe–O bond for the formation of a 7.3 kcal/mol more stable intermediate  $8_{\text{Fe}}$ . After a structural relaxation,  $8_{\text{Fe}}$  transforms to a 3.1 kcal/mol more stable intermediate  $9_{\text{Fe}}$ . Then a formaldehyde molecule is formed with the formation of the Fe–OBpin bond and the breaking of the Fe–OCH<sub>2</sub>OBpin and C–OBpin bonds through transition state  $\text{TS}_{9,10-\text{Fe}}$ . The dissociation of formaldehyde from  $10_{\text{Fe}}$  leaves an 8.6 kcal/mol more stable intermediate  $11_{\text{Fe}}$ . Then, another HBpin molecule approaches  $11_{\text{Fe}}$  and forms a 10.9 kcal/mol more stable intermediate  $12_{\text{Fe}}$  with the formation of a B–O bond. The dissociation of newly formed pinBOBpin molecule from  $12_{\text{Fe}}$  for the regeneration of the catalyst  $1_{\text{Fe}}$  is 9.5 kcal/mol uphill.

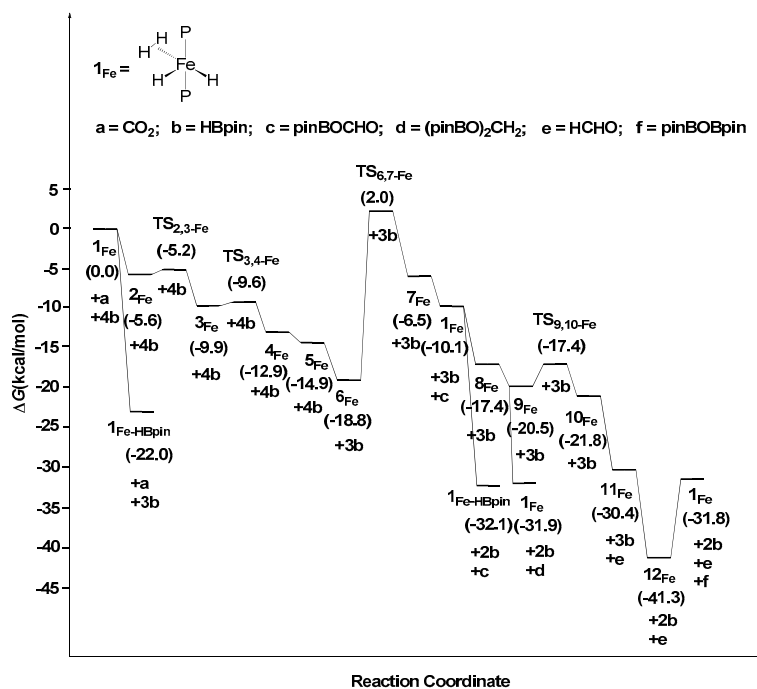


Figure 3. Free energies profile of the reduction of carbon dioxide to formaldehyde catalyzed by  $1_{\text{Fe}}$ .

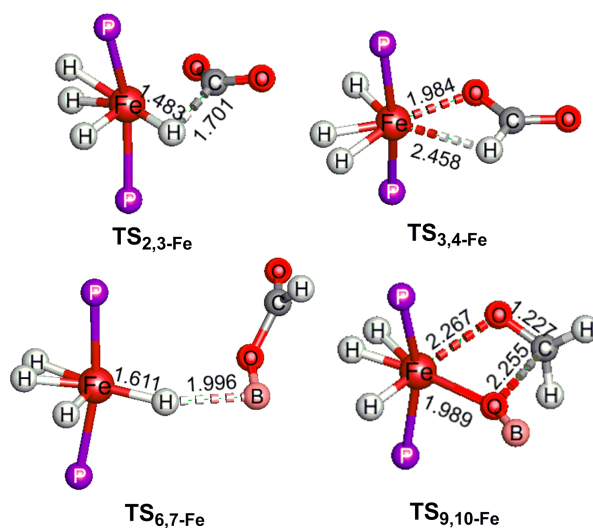


Figure 4. Optimized structures of  $\text{TS}_{2,3-\text{Fe}}$  ( $460i\text{ cm}^{-1}$ ),  $\text{TS}_{3,4-\text{Fe}}$  ( $78i\text{ cm}^{-1}$ ),  $\text{TS}_{6,7-\text{Fe}}$  ( $191i\text{ cm}^{-1}$ ) and  $\text{TS}_{9,10-\text{Fe}}$  ( $86i\text{ cm}^{-1}$ ). Bond lengths are in Å. The cyclopentyl and pinacol groups are not shown for clarity.

By comparing all relative free energies shown in Figure 3, we can conclude that  $1_{\text{Fe-HBpin}}$  and  $\text{TS}_{6,7-\text{Fe}}$  are the rate-determining states of the catalytic reaction with a total free energy barrier of 24.0 kcal/mol, which is 0.2 kcal/mol lower than the free energy barrier of the reaction catalyzed by  $1_{\text{Ru}}$ . Therefore,  $1_{\text{Fe}}$  is a potential low-cost and high efficiency catalyst for the reduction of  $\text{CO}_2$  to formaldehyde.

Sabo-Etienne and Bontemps [26] recently reported the catalytic reduction of  $\text{CO}_2$  to bis(boryl)acetal and methoxyborane, with  $\text{Fe}(\text{H})_2(\text{dmpe})_2$  used as catalyst precursor, and pinacolborane used as the reductant. For  $1_{\text{Ru}}$ , only one oxygen atom of  $\text{CO}_2$  is abstracted, and  $\text{CO}_2$  transforms into  $\text{HCHO}$ . For  $\text{Fe}(\text{H})_2(\text{dmpe})_2$ , one oxygen atom of  $\text{CO}_2$  is abstracted at the reduction step, then the second oxygen atom is removed and  $\text{CO}_2$  is transformed to methylene. This illustrates that iron complexes can efficiently catalyze the reduction of  $\text{CO}_2$ .

### 2.3. The Mechanism for the Reduction of Carbon Dioxide to Formaldehyde Catalyzed by the Os Complex

The reaction catalyzed by  $1_{\text{Os}}$  also has similar pathways to the reaction catalyzed by  $1_{\text{Ru}}$  (see Scheme S1 on catalytic cycle for the reduction of carbon dioxide to formaldehyde catalyzed by  $1_{\text{Os}}$ ). Figure 5 shows the calculated relative free energies in the reaction catalyzed by  $1_{\text{Os}}$ . Figure 6 shows the optimized structures of  $\text{Os-1cyp}$ ,  $1_{\text{Os}}$ ,  $4_{\text{Os}}$ ,  $\text{TS}_{7,8-\text{Os}}$  and  $8_{\text{Os}}$ , in which the distances between the two hydrogen atoms (marked in Figure 6) are longer than those in corresponding Ru complexes. As shown in Figure 5, the rate-determining states in the reaction catalyzed by the osmium complex are  $1_{\text{Os-HBpin}}$  and  $\text{TS}_{2,3-\text{Os}}$  with a free energy barrier of 29.0 kcal/mol, which is 4.8 kcal/mol higher than the free energy barrier of the reaction catalyzed by  $1_{\text{Ru}}$ . Therefore,  $1_{\text{Os}}$  could also catalyze the reduction of carbon dioxide to formaldehyde under harsher conditions.

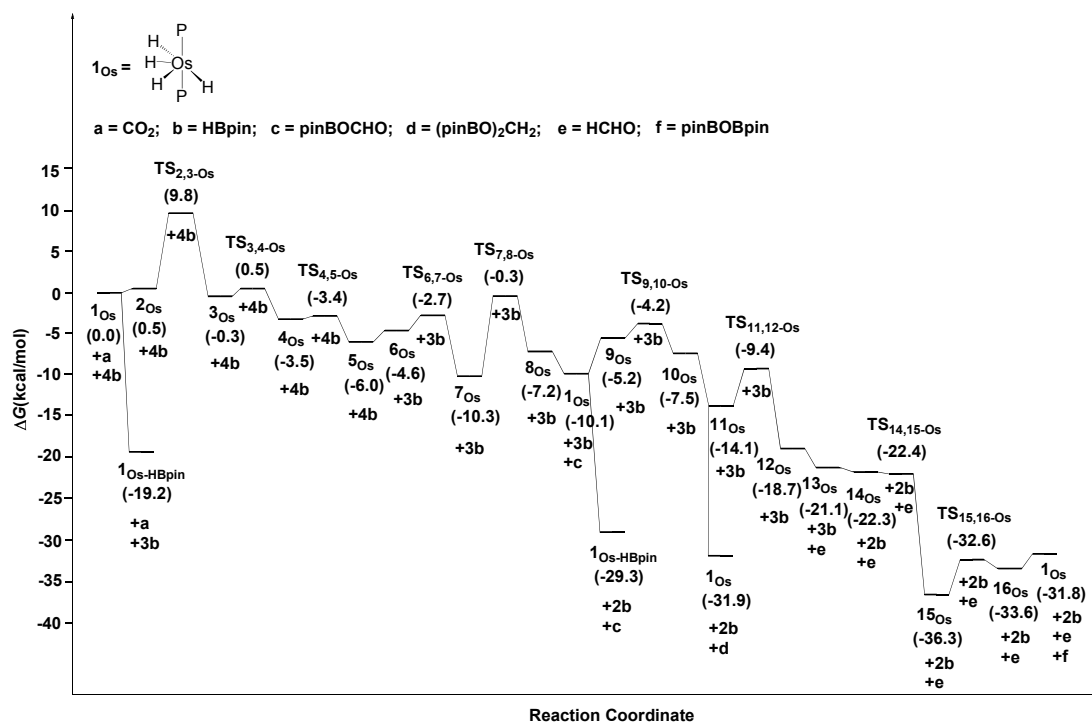
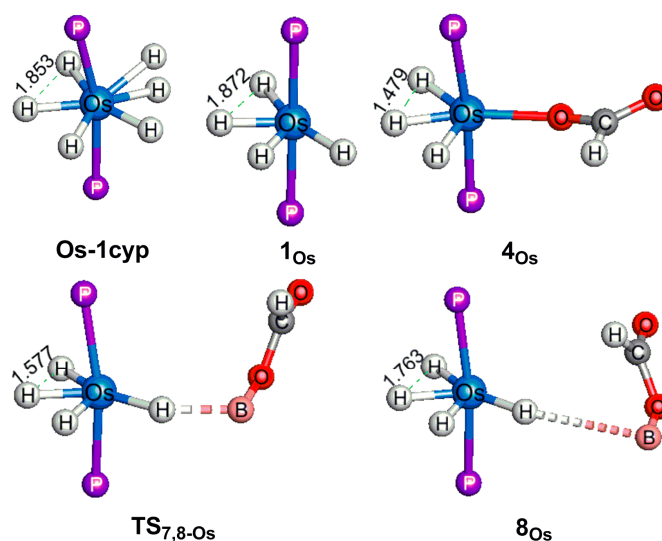


Figure 5. Free energies profile of the reduction of carbon dioxide to formaldehyde catalyzed by  $1_{\text{Os}}$ .



**Figure 6.** Optimized structures of **Os-1cyp**, **1<sub>Os</sub>**, **4<sub>Os</sub>**, **TS<sub>7,8-Os</sub>** (239i cm<sup>-1</sup>) and **8<sub>Os</sub>**. Bond lengths are in Å. The cyclopentyl and pinacol groups are not shown for clarity.

#### 2.4. Structures and Reactivity

According to our mechanistic study, the catalytic reaction of  $2\text{HBpin} + \text{CO}_2 \rightarrow \text{HCHO} + \text{pinBOBpin}$  has five stages,  $\text{CO}_2$  insertion (S1),  $\sigma$ -Bond metathesis (S2), pinBOCHO insertion (S3), HCHO elimination (S4) and  $\sigma$ -Bond metathesis (S5).

(S1)  $\text{CO}_2$  Insertion. The reaction in S1 is  $[\text{M}]-\text{H} + \text{CO}_2 \rightarrow [\text{M}]-\text{OOCH}$ . The most significant structural change in S1 is the cleavage of M–H bond. Table 1 lists the natural population analysis (NPA) charges of metal atoms ( $e$ ), the Wiberg bond indices (WBIs) of the bonds, and the relative free energies between intermediates and transition states/intermediates ( $\Delta G^\ddagger/\Delta G^\circ$ ) in stages. We can see that **2<sub>Fe</sub>** has the most negative NPA charge, the smallest WBI of the M–H bond and the lowest barrier for the cleavage of M–H bond among these three intermediates in S1.

(S2)  $\sigma$ -Bond Metathesis. The reaction in S2 is  $[\text{M}]-\text{OOCH} + \text{HBpin} \rightarrow [\text{M}]-\text{H} + \text{pinBOCHO}$ . The most important structural change in S2 is the cleavage of M–O bond. We can see **TS<sub>7,8-Os</sub>** has the least NPA charge, the smallest WBI of the M–O bond and the lowest barrier for the cleavage of M–O bond among these three transition states in S2.

(S3) pinBOCHO Insertion. The reaction in S3 is  $[\text{M}]-\text{H} + \text{pinBOCHO} \rightarrow [\text{M}]-\text{O}-\text{CH}_2-\text{OBpin}$ . The most important structural change in S3 is the M–H bond cleavage. **9<sub>Ru</sub>** has a more negative NPA charge, a smaller WBI of the M–H bond and a lower barrier for the cleavage of M–H bond than **9<sub>Os</sub>** in S3. The Fe complexes cannot be compared with the Ru and Os complexes because they have a different pathway in S3. Scheme 1 shows that **1<sub>Ru</sub>** and pinBOCHO first generate the intermediate **9<sub>Ru</sub>**, then form the intermediate **10<sub>Ru</sub>** through **TS<sub>9,10-Ru</sub>**, in which a Ru–O bond is formed. However, as shown in Scheme 2, **1<sub>Fe</sub>** combines directly with pinBOCHO and transforms to intermediate **8<sub>Fe</sub>**, in which an Fe–O bond is formed.

(S4) HCHO Elimination. The reaction in S4 is  $[\text{M}]-\text{O}-\text{CH}_2-\text{OBpin} \rightarrow \text{HCHO} + [\text{M}]-\text{OBpin}$ . The most important structural change in S4 is the cleavage of the M–O bond. **TS<sub>9,10-Fe</sub>** has the lowest barrier and the smallest WBI of the M–O bond among these three transition states in S4. There is no obvious relation between the energy barriers and the NPA charges of metal atoms in S4.

(S5)  $\sigma$ -Bond Metathesis. The reaction in S5 is  $[\text{M}]-\text{OBpin} + \text{HBpin} \rightarrow [\text{M}]-\text{H} + \text{pinBOBpin}$ . The most important structural change in S5 is the cleavage of the H–B bond. **15<sub>Os</sub>** has a smaller WBI of the H–B bond and a lower barrier for the cleavage of H–B bond than **15<sub>Ru</sub>** in S5. There is no obvious relation between the energy barriers and the NPA charges of metal atoms in S5. The Fe complexes cannot be compared with the Ru and Os complexes because they have a different pathway in S5.

**Table 1.** The natural population analysis (NPA) charges of metal atoms ( $e$ ), the Wiberg bond indices (WBIs) of the bonds, the relative free energies between intermediates and transition states/intermediates ( $\Delta G^\ddagger/\Delta G^\circ$ ).

Stages	Complexes	$e$	Bond	WBI	$\Delta G^\ddagger/\Delta G^\circ$ (kcal/mol)
Stage 1	2 <sub>Fe</sub>	−1.892	M–H bond	0.5876	0.4
	TS <sub>2,3-Fe</sub>	−1.782		0.5420	
	2 <sub>Ru</sub>	−1.538		0.6273	5.5
	TS <sub>2,3-Ru</sub>	−1.439		0.4674	
	2 <sub>Os</sub>	−1.540		0.6887	9.3
	TS <sub>2,3-Os</sub>	−1.518		0.5094	
Stage 2	6 <sub>Fe</sub>	−1.209	M–O bond	0.3517	20.8
	TS <sub>6,7-Fe</sub>	−0.974		0.0287	
	7 <sub>Ru</sub>	−1.411		0.2704	12.2
	TS <sub>7,8-Ru</sub>	−1.104		0.0275	
	7 <sub>Os</sub>	−1.427		0.2995	10.0
	TS <sub>7,8-Os</sub>	−1.111		0.0271	
Stage 3	1 <sub>Fe</sub>	−1.280	M–H bond	0.7154	−7.3
	8 <sub>Fe</sub>	−1.279		0.2182	
	9 <sub>Ru</sub>	−1.867		0.6661	0.5
	TS <sub>9,10-Ru</sub>	−1.850		0.5757	
	9 <sub>Os</sub>	−1.832		0.7206	1.0
	TS <sub>9,10-Os</sub>	−1.808		0.6002	
Stage 4	9 <sub>Fe</sub>	−0.890	M–O bond	0.4354	3.1
	TS <sub>9,10-Fe</sub>	−0.840		0.2609	
	11 <sub>Ru</sub>	−1.190		0.2583	3.8
	TS <sub>11,12-Ru</sub>	−1.184		0.2616	
	11 <sub>Os</sub>	−1.177		0.4049	4.7
	TS <sub>11,12-Os</sub>	−1.193		0.3061	
Stage 5	11 <sub>Fe</sub>	−0.778	/	/	−10.9
	12 <sub>Fe</sub>	−1.290		0.5236	
	15 <sub>Ru</sub>	−1.478	H–B bond	0.5325	4.5
	TS <sub>15,16-Ru</sub>	−1.795		0.0863	
	15 <sub>Os</sub>	−1.483		0.4898	3.7
	TS <sub>15,16-Os</sub>	−1.742		0.0958	

Overall, the above comparison of the important elementary steps of the reactions catalyzed by different metal complexes indicate that the smaller corresponding WBIs of bonds, and the lower energy barriers. We believe the reaction energy barriers are influenced by many factors. Due to the structural complexity of the transition metal complexes, the reaction energy barrier is not only decided by the electronic effect, but also relates to the sizes of metals, the binding strengths between metals and ligands, and the steric effects.

### 3. Computational Details

All DFT calculations were performed using the Gaussian 09 suite of programs [27] for the  $\omega$ B97X-D functional [28,29] with the Stuttgart relativistic effective core potential and associated valence basis sets for Ru (ECP28MWB, (8s7p6d2f1g)/[6s5p3d2f1g]) and Os (ECP60MWB, (8s7p6d2f1g)/[6s5p3d2f1g]) [30,31], all-electron 6-31++G(d,p) basis set for Fe, the atoms coordinated to metal atoms and the atoms in the reactant, and the 6-31G(d) basis set for all other atoms [32–34]. The  $\omega$ B97X-D functional was also used in the previous theoretical modeling of hydrogenation of

carbon dioxide by Fe complex [35] and the hydrogenation of dimethyl carbonate by Ru and Fe complexes [36]. The calculation results in those studies are in agreement with the experimental observations. In addition, high-level ab initio coupled cluster calibration study shows that  $\omega$ B97X-D performs well in barrier calculation of  $\sigma$ -bond activation promoted by Ru [37] and Fe [38] complexes. All structures reported in this paper were fully optimized with solvent effect corrections using the cavity-dispersion-solvent-structure terms in Truhlar and co-workers' SMD solvation model for benzene ( $\epsilon = 2.2706$ ) [39]. Tables and an xyz file giving solvent effect corrected absolute free energies, electronic energies and atomic coordinates of all optimized structures are given in Supporting Information. The thermal corrections were calculated at 298.15 K and 1 atm pressure with harmonic approximation. An ultrafine integration grid (99, 590) was used for numerical integrations. The ground states of intermediates and transition states were confirmed as singlets through a comparison with the optimized high-spin analogues. Calculating the harmonic vibrational frequencies for optimized structures and noting the number of imaginary frequencies (IFs) confirmed the nature of all intermediates (no IF) and transition state structures (only one IF for each transition state). The latter were also confirmed to connect reactants and products by intrinsic reaction coordinate (IRC) calculations. The 3D molecular structure figures displayed in this paper were drawn by using the JIMP2 molecular visualizing and manipulating program [40]. The NPA charges [41] and Wiberg indices [42] were obtained by using the NBO 3.1 program.

#### 4. Conclusions

In summary, the mechanistic insights of the reduction of carbon dioxide to formaldehyde catalyzed by Ru, Fe and Os complexes are investigated by using DFT. The formation of C–H and Ru–O bonds ( $\text{TS}_{9,10\text{-Ru}}$ ), the cleavage of Fe–O bond and the formation of O–B bond ( $\text{TS}_{6,7\text{-Fe}}$ ), and the formation of C–H bond ( $\text{TS}_{2,3\text{-Os}}$ ) are the rate-determining steps in the reactions catalyzed by the Ru, Fe, and Os complexes with total free energy barriers of 24.2 ( $\mathbf{1}_{\text{Ru-HBpin}} \rightarrow \text{TS}_{9,10\text{-Ru}}$ ), 24.0 ( $\mathbf{1}_{\text{Fe-HBpin}} \rightarrow \text{TS}_{6,7\text{-Fe}}$ ) and 29.0 ( $\mathbf{1}_{\text{Os-HBpin}} \rightarrow \text{TS}_{2,3\text{-Os}}$ ) kcal/mol, respectively. Such barriers indicate that  $\mathbf{1}_{\text{Fe}}$  is a potential low-cost catalyst for the reduction of carbon dioxide to formaldehyde under mild conditions. With all of our computational studies, we expect to predict the effects of different metals on the reaction and provide useful information for the development of base metal complexes for the conversion and utilization of carbon dioxide.

**Supplementary Materials:** Additional Supporting Information (Tables and an xyz file giving solvent effect corrected absolute free energies, electronic energies and atomic coordinates of all optimized structures; Scheme on catalytic cycle for the reduction of carbon dioxide to formaldehyde catalyzed by  $\mathbf{1}_{\text{Os}}$ ) are available online at [www.mdpi.com/2073-4344/7/1/5/s1](http://www.mdpi.com/2073-4344/7/1/5/s1).

**Acknowledgments:** X.Y. acknowledges financial support from the 100-Talent Program of the Chinese Academy of Sciences (CAS), and the National Natural Science Foundation of China (NSFC, 21373228, 21673250). H.C. is supported by the NSFC (21290194, 21473215). C.D. is grateful for the financial support from Natural Science Program of Handan University (16217).

**Author Contributions:** Xinzhen Yang and Chunhua Dong conceived and designed the computations; Chunhua Dong performed the computations; Chunhua Dong, Mingsong Ji, Hui Chen and Jiannian Yao analyzed the data; Chunhua Dong and Xinzhen Yang wrote the paper.

**Conflicts of Interest:** The authors declare no conflict of interest.

#### References

1. Kleeberg, C.; Cheung, M.S.; Lin, Z.; Marder, T.B. Copper-mediated reduction of  $\text{CO}_2$  with pinB-SiMe<sub>2</sub>Ph via  $\text{CO}_2$  insertion into a coppersilicon bond. *J. Am. Chem. Soc.* **2011**, *133*, 19060–19063. [[CrossRef](#)] [[PubMed](#)]
2. Rezayee, N.M.; Huff, C.A.; Sanford, M.S. Tandem amine and ruthenium-catalyzed hydrogenation of  $\text{CO}_2$  to methanol. *J. Am. Chem. Soc.* **2015**, *137*, 1028–1031. [[CrossRef](#)] [[PubMed](#)]
3. Bontemps, S.; Vendier, L.; Sabo-Etienne, S. Ruthenium-catalyzed reduction of carbon dioxide to formaldehyde. *J. Am. Chem. Soc.* **2014**, *136*, 4419–4425. [[CrossRef](#)] [[PubMed](#)]

4. LeBlanc, F.A.; Piers, W.E.; Parvez, M. Selective hydrosilation of CO<sub>2</sub> to a bis(silylactal) using an anilido bipyridyl-ligated organoscandium catalyst. *Angew. Chem. Int. Ed.* **2014**, *126*, 789–792. [[CrossRef](#)] [[PubMed](#)]
5. Moret, S.; Dyson, P.J.; Laurency, G. Direct synthesis of formic acid from carbon dioxide by hydrogenation in acidic media. *Nat. Commun.* **2014**, *5*, 4017. [[CrossRef](#)] [[PubMed](#)]
6. Brown, N.J.; Harris, J.E.; Yin, X.; Silverwood, I.; White, A.J.P.; Kazarian, S.G.; Hellgardt, K.; Shaffer, M.S.P.; Williams, C.K. Mononuclear phenolate diamine zinc hydride complexes and their reactions With CO<sub>2</sub>. *Organometallics* **2014**, *33*, 1112–1119. [[CrossRef](#)] [[PubMed](#)]
7. Dong, C.; Yang, X.; Yao, J.; Chen, H. Mechanistic study and ligand design for the formation of zinc formate complexes from zinc hydride complexes and carbon dioxide. *Organometallics* **2015**, *34*, 121–126. [[CrossRef](#)]
8. Tlili, A.; Blondiaux, E.; Frogneux, X.; Cantat, T. Reductive functionalization of CO<sub>2</sub> with amines: An entry to formamide, formamidine and methylamine derivatives. *Green Chem.* **2015**, *17*, 157–168. [[CrossRef](#)]
9. Berkefeld, A.; Piers, W.E.; Parvez, M.; Castro, L.; Maron, L.; Eisenstein, O. Decamethylscandocinium-hydrido-(perfluorophenyl)-borate: Fixation and tandem tris(perfluorophenyl)-borane catalysed deoxygenative hydrosilation of carbon dioxide. *Chem. Sci.* **2013**, *4*, 2152–2162. [[CrossRef](#)]
10. Li, Y.; Yan, T.; Junge, K.; Beller, M. Catalytic methylation of C–H bonds using CO<sub>2</sub> and H<sub>2</sub>. *Angew. Chem. Int. Ed.* **2014**, *53*, 10476–10480. [[CrossRef](#)] [[PubMed](#)]
11. Filonenko, G.A.; Smykowski, D.; Szyja, B.M.; Li, G.N.; Szczygiel, J.; Hensen, E.J.M.; Pidko, E.A. Catalytic hydrogenation of CO<sub>2</sub> to formates by a lutidine-derived Ru-CNC pincer complex: Theoretical insight into the unrealized potential. *ACS Catal.* **2015**, *5*, 1145–1154. [[CrossRef](#)]
12. Haunschild, R. Theoretical study on the reaction mechanism of carbon dioxide reduction to methanol using a homogeneous ruthenium(II) phosphine catalyst. *Polyhedron* **2015**, *85*, 543–548. [[CrossRef](#)]
13. Musashi, Y.; Sakaki, S. Theoretical study of ruthenium-catalyzed hydrogenation of carbon dioxide into formic acid. Reaction mechanism involving a new type of sigma-bond metathesis. *J. Am. Chem. Soc.* **2000**, *122*, 3867–3877. [[CrossRef](#)]
14. Chong, C.C.; Kinjo, R. Catalytic hydroboration of carbonyl derivatives, imines, and carbon dioxide. *ACS Catal.* **2015**, *5*, 3238–3259. [[CrossRef](#)]
15. Bontemps, S. Boron-mediated activation of carbon dioxide. *Coord. Chem. Rev.* **2015**, *308*, 117–130. [[CrossRef](#)]
16. Suh, H.-W.; Guard, L.M.; Hazari, N. A mechanistic study of allene carboxylation with CO<sub>2</sub> resulting in the development of a Pd(II) pincer complex for the catalytic hydroboration of CO<sub>2</sub>. *Chem. Sci.* **2014**, *5*, 3859–3872. [[CrossRef](#)]
17. Courtemanche, M.-A.; Légaré, M.-A.; Maron, L.; Fontaine, F.-G. Reducing CO<sub>2</sub> to methanol using frustrated lewis pairs: On the mechanism of phosphine–borane-mediated hydroboration of CO<sub>2</sub>. *J. Am. Chem. Soc.* **2014**, *136*, 10708–10717. [[CrossRef](#)] [[PubMed](#)]
18. Courtemanche, M.-A.; Légaré, M.-A.; Maron, L.; Fontaine, F.-G. A highly active phosphine–borane organocatalyst for the reduction of CO<sub>2</sub> to methanol using hydroboranes. *J. Am. Chem. Soc.* **2013**, *135*, 9326–9329. [[CrossRef](#)] [[PubMed](#)]
19. Declercq, R.; Bouhadir, G.; Bourissou, D.; Légaré, M.-A.; Courtemanche, M.-A.; Nahi, K.S.; Bouchard, N.; Fontaine, F.-G.; Maron, L. Hydroboration of carbon dioxide using ambiphilic phosphine–borane catalysts: On the role of the formaldehyde adduct. *ACS Catal.* **2015**, *5*, 2513–2520. [[CrossRef](#)]
20. Lu, Z.; Hausmann, H.; Becker, S.; Wegner, H.A. Aromaticity as stabilizing element in the bidentate activation for the catalytic reduction of carbon dioxide. *J. Am. Chem. Soc.* **2015**, *137*, 5332–5335. [[CrossRef](#)] [[PubMed](#)]
21. Huang, F.; Zhang, C.; Jiang, J.; Wang, Z.-X.; Guan, H. How does the nickel pincer complex catalyze the conversion of CO<sub>2</sub> to a methanol derivative? A computational mechanistic study. *Inorg. Chem.* **2011**, *50*, 3816–3825. [[CrossRef](#)] [[PubMed](#)]
22. Suh, H.-W.; Guard, L.M.; Hazari, N. Synthesis and reactivity of a masked PSiP pincer supported nickel hydride. *Polyhedron* **2014**, *84*, 37–43. [[CrossRef](#)]
23. Anker, M.D.; Arrowsmith, M.; Bellham, P.; Hill, M.S.; Kociok-Kohn, G.; Liptrot, D.J.; Mahon, M.F.; Weetman, C. Selective reduction of CO<sub>2</sub> to a methanol equivalent by B(C<sub>6</sub>F<sub>5</sub>)<sub>3</sub>-activated alkaline earth catalysis. *Chem. Sci.* **2014**, *5*, 2826–2830. [[CrossRef](#)]
24. Sypaseuth, F.D.; Matlachowski, C.; Weber, M.; Schwalbe, M.; Tzschucke, C.C. Electrocatalytic carbon dioxide reduction by using cationic pentamethylcyclopentadienyl-iridium complexes with unsymmetrically substituted bipyridine ligands. *Chem.–Eur. J.* **2015**, *21*, 6564–6571. [[CrossRef](#)] [[PubMed](#)]

25. Glendening, E.D.; Reed, A.E.; Carpenter, J.E.; Weinhold, F. *NBO Version 3.1*; TCI, University of Wisconsin: Madison, WI, USA, 1998.
26. Jin, G.; Werncke, C.G.; Escudié, Y.; Sabo-Etienne, S.; Bontemps, S. Iron-catalyzed reduction of CO<sub>2</sub> into methylene: Formation of C–N, C–O, and C–C bonds. *J. Am. Chem. Soc.* **2015**, *137*, 9563–9566. [[CrossRef](#)] [[PubMed](#)]
27. Frisch, M.J.; Trucks, G.W.; Schlegel, H.B.; Scuseria, G.E.; Robb, M.A.; Cheeseman, J.R.; Scalmani, G.; Barone, V.; Mennucci, B.; Petersson, G.A.; et al. *Gaussian 09, Revision C.01*; Gaussian, Inc.: Wallingford, CT, USA, 2010.
28. Chai, J.-D.; Head-Gordon, M. Systematic optimization of long-range corrected hybrid density functionals. *J. Chem. Phys.* **2008**, *128*, 084106. [[CrossRef](#)] [[PubMed](#)]
29. Chai, J.-D.; Head-Gordon, M. Long-range corrected hybrid density functionals with damped atom–atom dispersion corrections. *Phys. Chem. Chem. Phys.* **2008**, *10*, 6615–6620. [[CrossRef](#)] [[PubMed](#)]
30. Andrae, D.; Häußermann, U.; Dolg, M.; Stoll, H.; Preuß, H. Energy-adjusted ab initio pseudopotentials for the second and third row transition elements. *Theor. Chim. Acta* **1990**, *77*, 123–141. [[CrossRef](#)]
31. Martin, J.M.L.; Sundermann, A. Correlation consistent valence basis sets for use with the Stuttgart–Dresden–Bonn relativistic effective core potentials: The atoms Ga–Kr and In–Xe. *J. Chem. Phys.* **2001**, *114*, 3408–3420. [[CrossRef](#)]
32. Hehre, W.J.; Ditchfield, R.; Pople, J. Self-consistent molecular orbital methods. XII. Further extensions of Gaussian-type basis sets for use in molecular orbital studies of organic molecules. *J. Chem. Phys.* **1972**, *56*, 2257–2261. [[CrossRef](#)]
33. Hariharan, P.C.; Pople, J.A. The influence of polarization functions on molecular orbital hydrogenation energies. *Theor. Chim. Acta* **1973**, *28*, 213–222. [[CrossRef](#)]
34. Krishnan, R.; Binkley, J.S.; Seeger, R.; Pople, J.A. Self-consistent molecular orbital methods. XX. A basis set for correlated wave functions. *J. Chem. Phys.* **1980**, *72*, 650–654. [[CrossRef](#)]
35. Yang, X. Hydrogenation of carbon dioxide catalyzed by PNP pincer iridium, iron, and cobalt complexes: A computational design of base metal catalysts. *ACS Catal.* **2011**, *1*, 849–854. [[CrossRef](#)]
36. Yang, X. Metal hydride and ligand proton transfer mechanism for the hydrogenation of dimethyl carbonate to methanol catalyzed by a pincer ruthenium complex. *ACS Catal.* **2012**, *2*, 964–970. [[CrossRef](#)]
37. Sun, Y.; Hu, L.; Chen, H. Comparative assessment of DFT performances in Ru- and Rh-promoted  $\sigma$ -bond activations. *J. Chem. Theory Comput.* **2015**, *11*, 1428–1438. [[CrossRef](#)] [[PubMed](#)]
38. Sun, X.; Sun, X.; Geng, C.; Zhao, H.; Li, J. Benchmark study on methanol C–H and O–H bond activation by bare [Fe<sup>IV</sup>O]<sup>2+</sup>. *J. Phys. Chem. A* **2014**, *118*, 7146–7158. [[CrossRef](#)] [[PubMed](#)]
39. Marenich, A.V.; Cramer, C.J.; Truhlar, D.G. Universal solvation model based on solute electron density and on a continuum model of the solvent defined by the bulk dielectric constant and atomic surface tensions. *J. Phys. Chem. B* **2009**, *113*, 6378–6396. [[CrossRef](#)] [[PubMed](#)]
40. Manson, J.; Webster, C.E.; Hall, M.B. *JIMP2, Version 0.091, a Free Program for Visualizing and Manipulating Molecules*; Texas A&M University: College Station, TX, USA, 2006.
41. Reed, A.E.; Weinstock, R.B.; Weinhold, F. Natural population analysis. *J. Chem. Phys.* **1985**, *83*, 735–746. [[CrossRef](#)]
42. Wiberg, K.B. Application of the pople-santry-segal CNDO method to the cyclopropylcarbonyl and cyclobutyl cation and to bicyclobutane. *Tetrahedron* **1968**, *24*, 1083–1096. [[CrossRef](#)]

